J Solid State Electrochem (2012) 16:587–595
DOI 10.1007/s10008-011-1389-5

ORIGINAL PAPER

Oxidation of carbon monoxide and formic acid on bulk and nanosized Pt–Co alloys

Maja D. Obradović · Amalija V. Tripković · Snežana Lj. Gojković

Received: 10 December 2010 / Revised: 25 March 2011 / Accepted: 26 March 2011 / Published online: 20 April 2011

Abstract Bulk Pt_3Co and nanosized Pt_3Co and PtCo alloys supported on high area carbon were investigated as the electrocatalysts for the CO_{ads} and HCOOH oxidation. Pt_3Co alloy with Co electrochemically leached from the surface (Pt skeleton) was employed to separate electronic from ensemble and bifunctional effects of Co. Cyclic voltammetry in 0.1 M $HClO_4$ showed reduced amount of adsorbed hydrogen on Pt sites on Pt_3Co alloy compared to pure Pt. However, no significant difference in hydrogen adsorption/desorption and Pt-oxide reduction features between Pt_3Co with Pt skeleton structure and bulk Pt was observed. The oxidation of CO_{ads} on Pt_3Co alloy commenced earlier than on Pt, but this effect on Pt_3Co with Pt skeleton structure was minor indicating that bifunctional mechanism is stronger than the electronic modification of Pt by Co. The HCOOH oxidation rate on Pt_3Co alloy was about seven times higher than on bulk Pt when the reaction rates were compared at 0.4 V, i.e., in the middle of the potential range for the HCOOH oxidation. Like in the case of CO_{ads} oxidation, Pt skeleton showed similar activity as bulk Pt indicating that the ensemble effect is responsible for the enhanced activity of Pt_3Co alloy toward HCOOH oxidation. The comparison of CO_{ads} and HCOOH oxidation on Pt_3Co/C and PtCo/C with the same reaction on Pt/C were qualitatively the same as on bulk materials.

M. D. Obradović · A. V. Tripković
Institute of Chemistry, Technology and Metallurgy,
University of Belgrade,
Njegoševa 12,
11000 Belgrade, Serbia

S. L. Gojković (✉)
Faculty of Technology and Metallurgy, University of Belgrade,
Karnegijeva 4,
11000 Belgrade, Serbia
e-mail: sgojkovic@tmf.bg.ac.rs

Keywords Platinum–cobalt alloy · Formic acid · Carbon monoxide · Electrochemical oxidation · Electronic effect · Ensemble effect

Introduction

Small polymer electrolyte membrane fuel cells (PEMFC) as portable power generators offer several advantages over conventional batteries. Because of difficulties in storage and handling of gaseous hydrogen, organic liquids such as methanol and formic acid are considered as potential fuels in PEMFC for this type of application. Advantage of HCOOH over CH_3OH is its lower crossover through Nafion® membrane, allowing the use of highly concentrated fuel solutions and thinner membranes in direct formic acid fuel cell (DFAFC) than in direct methanol fuel cell. Also, HCOOH is somewhat less toxic than CH_3OH and equilibrium voltage of O_2/HCOOH cell is higher than O_2/CH_3OH cell (1.48 versus 1.213 V) [1].

It is generally accepted that HCOOH oxidizes to CO_2 via a dual path mechanism [2]. Direct path is dehydrogenation of HCOOH molecule without forming CO_{ads}:

$$HCOOH \rightarrow CO_2 + 2H^+ + 2e^-$$

A reactive intermediate in this reaction is likely to be formate species, HCOO [3]. Indirect path comprises dehydration of HCOOH molecule with the formation of CO_{ads} and its further oxidation to CO_2:

$$HCOOH \rightarrow CO_{ads} + H_2O \rightarrow CO_2 + 2H^+ + 2e^-$$

At low potentials CO_{ads} cannot be oxidized on Pt and it acts as the catalyst poison. Since low potentials are crucial

for high power performance of DFAFC, the presence of CO_{ads} on the anode surface is to be avoided or at least greatly reduced. This can be achieved by combining Pt with some other metal performing its role through (a) bifunctional mechanism, (b) electronic effect, or (c) ensemble or third-body effect.

Bifunctional mechanism is operative when the second metal is capable to adsorb oxygen-containing species at lower potentials than Pt, so that CO_{ads} formed through HCOOH dehydration on Pt sites is oxidized by oxygen-containing species on the other metal sites. Electronic effect refers to the modification of the electronic structure of Pt atoms, generally resulting in change of the adsorption ability of Pt. If this modification weakens the bond between Pt and CO_{ads}, the electronic effect reduces Pt poisoning. The ensemble or third-body effect is based on the fact that the dehydration path requires at least three contiguous Pt atoms, whereas the dehydrogenation path requires at most two Pt atoms [4, 5]. Therefore, when large Pt surface is interrupted by foreign atoms, dehydrogenation path is favored and CO_{ads} formation is suppressed.

The activity of Pt towards HCOOH oxidation is greatly improved by the addition of Au [6–10]. We have shown recently [11] that the high activity of Pt–Au surfaces arises from the ensemble effect, which can enhance the reaction rate by two orders of magnitude and eliminate poisoning by CO_{ads} if Pt fraction on the catalyst surface is low. In other bimetallic systems, like Pt–Pb [12, 13], Pt–Bi [14, 15], Pt–Sn [16], Pt–Mo [17], and Pt–Pd [18, 19], the electronic and bifunctional effects were also considered. Interestingly, HCOOH oxidation has not been studied on Pt modified by 3*d* transition metals. In our opinion, these systems deserve attention because 3*d* transition metals possess two characteristics that can be beneficial for Pt activity. They are oxidized at lower potential than Pt, meaning that HCOOH oxidation can occur through bifunctional mechanism. Also, the electronic modification of Pt by 3*d* transition metals due to both ligand [20] and strain effect [21] produces lowering of 3*d* band center of Pt. This reduces electron back-donation from Pt to the adsorbates, such as CO, and weakens the bond between them.

In this work we present the results of the CO_{ads} and HCOOH oxidation on bulk and nanosized Pt–Co alloys. These catalysts exhibited higher activity for oxygen reduction than Pt, even if Co was removed from the surface of the electrocatalyst, which was ascribed to the inhibition of Pt-OH_{ads} formation on Pt sites electronically modified by Co atoms in subsurface layers [22, 23]. The investigation of CO adsorption on Pt and Pt–Co alloy using X-ray photoelectron spectroscopy measurements combined with an electrochemical cell (EC-XPS) showed that CO binds more weakly to the Pt sites of the alloy than to pure Pt [24]. Therefore, we postulated that, along with the ensemble effect, which is purely geometric and should be exhibited by any foreign atom, Co can promote HCOOH oxidation through the bifunctional mechanism and the electronic effect.

In the investigation we used Pt_3Co bulk alloy and Pt_3Co/C and PtCo/C catalysts. Although Pourbaix diagram predicts dissolution of Co in acid environment because Co^{2+} is the stable species at the potentials over −0.4 V, there are experimental evidences [25, 26] that Pt–Co surfaces posses moderate stability in acid environment, i. e., that behavior of Co in Pt–Co alloys is different than that of pure Co. Bogdanovskaya et al. [25] investigated PtCo/C catalyst surface composition by XPS and demonstrated that after ~100 h in 0.5 M H_2SO_4 at 60 °C, fraction of Co on the surface decreased from 0.70 to 0.48. Also, Xu et al. [26] showed that potentiostating of PtCo thin layer in the hydrogen adsorption/desorption region and in the double-layer region does not induce Co leaching. Therefore, we assumed that chemical dissolution of Co during the electrochemical measurements is negligible. The investigated catalysts were preconditioned electrochemically by: (a) the short potential cycling without electrochemical dissolution of Co and (b) the extensive potential cycling allowing complete electrochemical dissolution of Co from the surface, i.e., forming a Pt skeleton structure [27]. The aim of using skeleton structure was to separate the electronic effects of Co from the bifunctional and ensemble effects which are operative only if both Pt and Co are in the contact with electrolyte. Also, the skeleton structure is representative for the state of the Pt–Co and alike catalysts during long-term operation of the fuel cell, during which Co is depleted not only from topmost layer but from up to the 5-nm thick layer of the Pt–Co alloy [26].

Experimental

Polycrystalline Pt and Pt_3Co electrodes in the form of disc were used in this study. Pt_3Co alloy was prepared and characterized at Lawrence Berkeley National Laboratory, Berkeley, USA [22]. In short, the alloy was fabricated by arc melting of the pure elements in inert atmosphere in the proportion of Co to Pt=1:3. Bulk composition of the alloy, assessed via X-ray fluorescence spectroscopy, was confirmed to be c.a. 25 at percentage of Co. X-ray diffraction (XRD) showed the specimen to be single-phase fcc solid solution having the expected lattice constant for 75% Pt [22]. Prior to an electrochemical experiment, Pt and Pt_3Co electrodes were polished with an Al_2O_3 suspension (particle size 0.1 and 0.05 μm) and cleaned ultrasonically in high purity water.

Nanosized electrocatalysts were commercially available Pt, Pt_3Co, and PtCo (20 mass percent of total metal)

supported on Vulcan XC-72 carbon black, provided by E-TEK. These catalysts have also been characterized previously by XRD and transmission electron microscopy (TEM) [23]. XRD analysis of Pt_3Co and PtCo nanoalloys revealed a single fcc phase in each sample, with the lattice constant of 0.384 nm (Pt_3Co) and 0.374 (PtCo) that are in reasonable agreement with the lattice constant reported for the corresponding bulk solid solutions [23]. According to the TEM images, Pt_3Co and PtCo particles are well dispersed on carbon black support and their diameters are 3.4±0.7 and 4.4±2.6 nm, respectively [23].

For the electrochemical measurements, the Pt/C, Pt_3Co/C, and PtCo/C catalysts were applied onto gold substrate (4.5 mm in diameter) in the form of a thin layer. Catalyst powder was suspended in high purity water in the concentration of 2 mg cm^{-3}. In all cases, 50 μl of the Nafion® solution (5 wt.%, 1,100 E.W., Aldrich) was added per 1.0 cm^3 of the suspension, in order to insure the adhesion of the layer. After 1 h of agitation in an ultrasonic bath, 10 μl of the suspension was placed onto gold electrode and left to dry overnight. This procedure resulted in the total metal loading on the electrode of 25 μg cm^{-2}.

A three-compartment electrochemical glass cell with a Pt wire as the counter electrode and a saturated calomel electrode as the reference electrode was used. All the potentials reported in the paper are expressed on the scale of the reversible hydrogen electrode. The supporting electrolyte of 0.1 M $HClO_4$ (99.999% purity, Sigma-Aldrich) was prepared with high purity water (Millipore, 18 MΩ cm resistivity). The electrolyte was deaerated by the bubbling N_2. Electrochemical oxidation of HCOOH was investigated in deaerated supporting electrolyte containing 0.5 M HCOOH (Merck). In the positive-going scan, the potential was held at 0.10 V and HCOOH was added into the electrolyte. After 2 min the scan was continued at the rate of 1 mV s^{-1} (quasi steady-state measurements) or at 50 mV s^{-1} (potentiodynamic measurements). For the CO-stripping measurements, pure CO was bubbled through the electrolyte for 20 and 30 min while keeping the electrode potential at 0.12 and 0.10 V, for flat and high surface area Pt-based catalysts, respectively [7]. After purging the electrolyte by N_2 for 30 min to eliminate the dissolved CO, the adsorbed CO was oxidized in an anodic scan at 20 mV s^{-1}. Two subsequent voltammograms were also recorded to verify the completeness of the CO oxidation.

Real surface area of the bulk Pt electrode was determined from the hydrogen desorption charge corrected for the double-layer charging and assuming 210 μC cm^{-2} for monolayer hydrogen adsorption. This result was confirmed by the calculation of the charge of CO stripping (assuming 420 μC cm^{-2} for the CO monolayer). Electrochemical active surface area of Pt for the Pt–Co catalysts was calculated from the CO-stripping measurements.

The experiments were conducted at 298±0.5 K. A Pine RDE4 potentiostat and Philips PM 8143 X–Y recorder were employed.

Results and discussion

Voltammetry of bulk Pt_3Co electrode

Cyclic voltammogram of bulk Pt_3Co alloy recorded in 0.1 M $HClO_4$ solution is presented in Fig. 1a. The positive potential limit of 0.9 V was chosen to prevent electrochemical dissolution of Co, and according to the voltammogram, this process is avoided. The voltammogram of Pt electrode previously cycled within the same limits as Pt_3Co is also given in Fig. 1a. Neither voltammogram in Fig. 1a shows fully developed and resolved hydrogen adsorption/desorption peaks of Pt because such a feature can be obtained only after the potential cycling of Pt between the onset potentials of H_2 and O_2 evolution. Although the charge under the

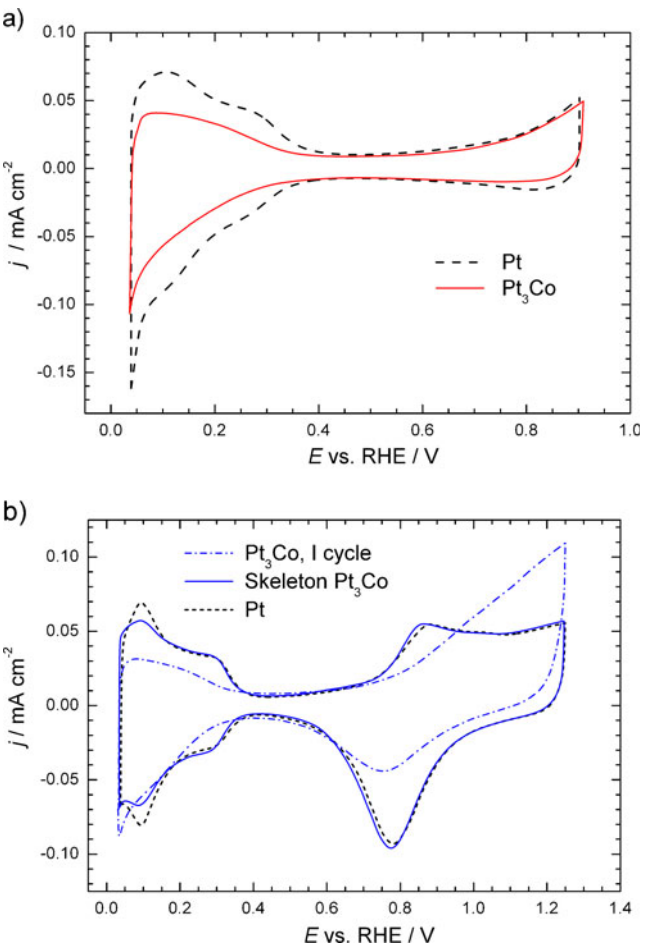

Fig. 1 Cyclic voltammograms of **a** bulk Pt and Pt_3Co alloy and **b** bulk Pt, Pt_3Co alloy, and Pt skeleton Pt_3Co structure recorded in 0.1 M $HClO_4$ at the sweep rate of 50 mV s^{-1}

peak for Pt_3Co electrode must be lower than the charge for pure Pt because hydrogen is not adsorbed on Co, it is still lower than expected for the surface having at least 75% of Pt. Low surface coverage of Pt sites on Pt_3Co electrode by adsorbed hydrogen might be attributed to the electronic modification of Pt by Co atoms, but as will be discussed below, this effect was not unambiguously proven in the case of OH and CO adsorption.

The first voltammogram of Pt_3Co electrode upon the extension of the positive potential limit is presented in Fig. 1b. The anodic current of Pt-oxide formation and possibly Co dissolution arose and the cathodic peak of Pt-oxide reduction appears. Over the potential cycling, the hydrogen adsorption/desorption peaks gradually increase and the onset potential for formation of Pt-oxide shifts negatively. Since the steady-state voltammogram of Pt_3Co alloy in the extended potential window is very close to the voltammogram of bulk Pt, also presented in Fig. 1b, it is supposed that Co is completely leached from the surface of the alloy, i.e., that Pt skeleton structure was formed. Comparison of these two voltammograms also shows that Co leaching form the Pt_3Co surface does not produce significant roughening of the electrode surface.

By contrasting the voltammograms of Pt_3Co electrode with Pt skeleton structure and the bulk Pt, one cannot find a clear evidence for the influence of the Co atoms from the subsurface layer on the adsorptive properties of Pt. The cathodic peak of Pt-oxide reduction on Pt skeleton surface is displaced with respect to this on bulk Pt for only 7 mV towards negative potentials, which would correspond to stronger adsorption of oxygen-containing species on the Pt skeleton surface. Concerning hydrogen adsorption, charge under the peaks at ~0.1 V, corresponding to the weakly adsorbed hydrogen at Pt(111) and Pt(110) planes [28], is slightly lower for the Pt skeleton surface than for bulk Pt. Although DFT calculations [20, 21] predict weaker bond between Pt and adsorbates in the presence of the early-transition metal underlayers, experimental evidences are not wholly straightforward. In the work of Stamenkovic et al. [22], the voltammograms of bulk Pt and annealed Pt_3Co electrode having Pt monolayer, i.e., Pt skin on the surface show reduced charge for weakly adsorbed hydrogen and facilitated reduction of Pt oxide on the Pt skin surface. However, the study of platinized cobalt coatings performed by Sotiropoulos and co-worker [29, 30] shows no difference in the hydrogen adsorption/desorption region with respect to Pt electrode. They also reported negative shift in the Pt-oxide reduction on the Pt atoms in contact with Co, indicating a higher coverage of oxygen-containing species. Watanabe and co-workers [31] investigated Pt–Fe alloy with the "Pt skeleton" structure. Their voltammograms showed no difference in Pt-oxide reduction peak while the peaks for weakly adsorbed hydrogen are slightly decreased with respect to pure Pt, similarly to our results. By using EC-XPS, they compared the coverage of "Pt skeleton" Pt–Fe alloy and pure Pt by H_2O_{ads}, OH_{ad}, and O_{ads} and found inhibition of H_2O_{ads} formation and promotion of O_{ads} formation by Fe, but no effect on OH_{ads} formation.

Oxidation of CO_{ads} on bulk Pt_3Co electrode

Real surface area of Pt is usually determined from the charge of hydrogen adsorption/desorption processes, but in the case of Pt_3Co bimetallic surface, this method can provide a false result for the reasons explained above. Thus, we employed the stripping of preadsorbed CO, assuming that Co is inactive for CO adsorption. In addition to the determination of the Pt surface area, this experiment gives insight in the kinetics of CO oxidation, which is a possible reaction step in HCOOH oxidation.

The stripping voltammograms of CO_{ads} were recorded on Pt, Pt_3Co, and the Pt skeleton Pt_3Co electrode. The results presented in Fig. 2a show that the onset potential of

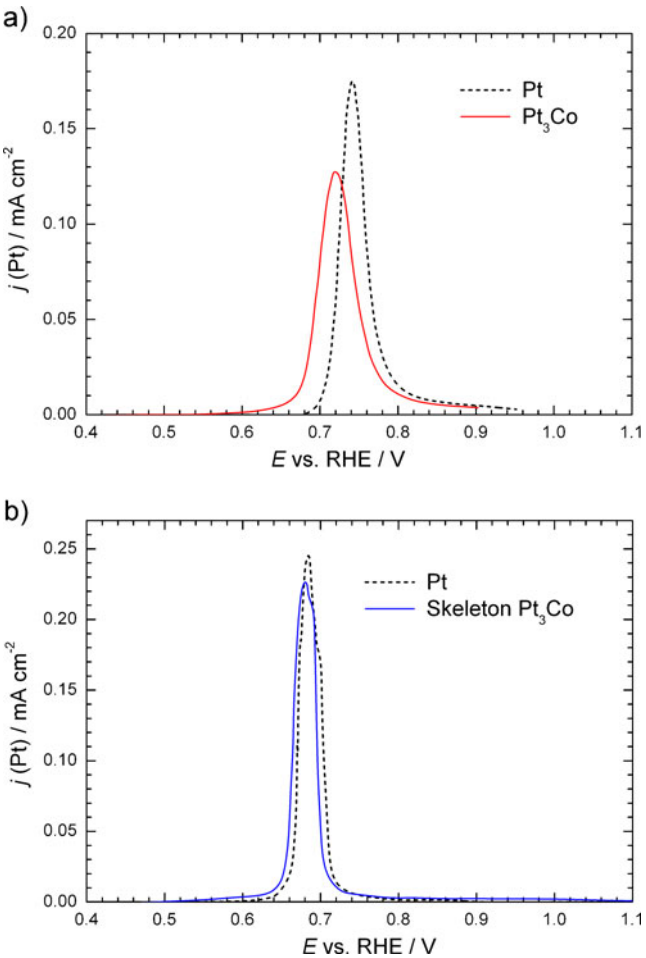

Fig. 2 CO_{ads} stripping voltammograms on **a** bulk Pt and Pt_3Co alloy and **b** bulk Pt and "Pt skeleton" Pt_3Co structure in 0.1 M $HClO_4$ recorded at the sweep rate of 20 mV s^{-1}

CO_{ads} oxidation on Pt_3Co is ~30 mV less positive than on pure Pt. This can be attributed to the weakened bond between Pt and CO_{ads}, but also to the facilitated CO_{ads} oxidation by the oxygen-containing species adsorbed on Co atoms. The difference between CO_{ads} stripping voltammograms on "Pt skeleton" Pt_3Co electrode and pure Pt (Fig. 2b) is minor with the negative shift of less than 10 mV for the Pt skeleton structure. This is similar to the result of Watanabe and co-workers [24] who found no difference in the potential of the main peak of CO_{ads} oxidation. Since Co atoms are leached from the surface of the Pt skeleton structure, small shift in CO_{ads} peak can be caused only by the electronic modification of Pt by Co atoms beneath the surface. Therefore, it seems that Co influences the oxidation of CO_{ads} on Pt–Co bimetallic surfaces more through the bifunctional mechanism than through the electronic modification of Pt.

The results displayed in Fig. 2 underline the effect of the Pt surface pretreatment on the CO_{ads} oxidation. The peak potential of the CO_{ads} stripping on the Pt previously cycled up to 0.9 V is 0.74 V, while on the Pt cycled up to 1.3 V, the peak potential is 0.68 V. Potential cycling of Pt introduces steps on its surface, which are known to preferentially adsorb OH species necessary for the CO_{ads} oxidation. Almost overlapping CO_{ads} stripping curves for Pt and Pt skeleton Pt_3Co surface (Fig. 2b) indicate that the Pt surface structure has greater influence on the CO_{ads} oxidation kinetics than the electronic modification of Pt by the Co atoms.

Oxidation of formic acid on bulk Pt_3Co electrode

Polarization curves for the oxidation of formic acid were recorded at Pt_3Co alloy and compared to those on Pt and Pt skeleton Pt_3Co structure. For all the electrodes, the current densities were calculated per Pt surface determined from CO_{ads} stripping. Potentiodynamic profiles presented in Fig. 3a correspond to HCOOH oxidation on Pt_3Co alloy and bulk Pt electrodes, both of which were previously cycled with the positive limit of 0.9 V. The curves display characteristic features of HCOOH oxidation: after reaching a plateau, the currents ascend and exhibit a peak at ~0.95 V. This means that at low potentials, HCOOH oxidizes through the direct path with the simultaneous formation of CO_{ads} through the indirect path [2, 32]. Increasing coverage of CO_{ads} reduces the amount of Pt surface available for the direct path, and so the current density reaches a plateau. Subsequent formation of oxygen-containing species on Pt enables the oxidative removal of CO_{ads}. As more Pt sites are being released, the HCOOH oxidation current increases until Pt oxide, inactive for HCOOH oxidation, is formed. Figure 3a shows that there is no significant difference in the onset potential for the Pt_3Co and bulk Pt, and that both

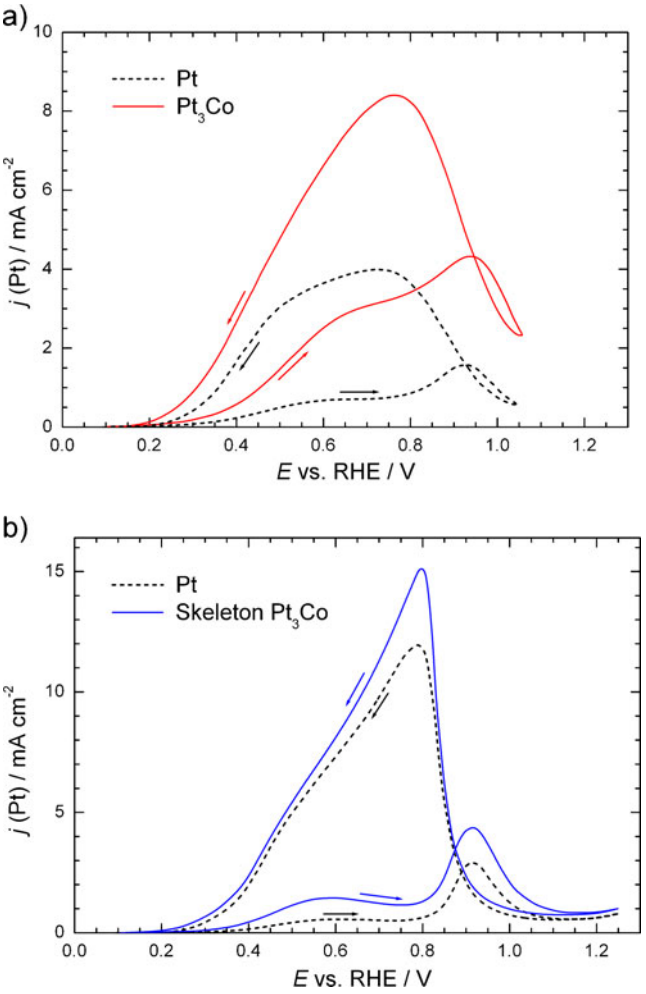

Fig. 3 Potentiodynamic polarization curves for the oxidation of HCOOH in 0.1 M $HClO_4$+0.5 M HCOOH electrolyte recorded on **a** bulk Pt and Pt_3Co alloy and on **b** bulk Pt and Pt skeleton Pt_3Co structure. Sweep rate 50 mV s^{-1}. Current densities are referred to Pt surface

curves exhibit the peak at ~0.95 V, i.e., they are poisoned by CO_{ads}. However, on the curve for Pt_3Co alloy, the peak is lower with respect to the plateau, indicating that on this surface, less CO_{ads} is formed than on pure Pt.

In Fig. 3b the potentiodynamic curves of HCOOH oxidation on the Pt_3Co electrode with Pt skeleton structure is compared to this on bulk Pt previously cycled in the same potential window as Pt_3Co alloy during the Co leaching (between 0.035 V and 1.25 V). On both surfaces the indirect path is predominant over the direct path and the coverage by CO_{ads} is substantial. Pt skeleton Pt_3Co structure performs better than bulk Pt, but bulk Pt_3Co alloy exhibits the higher activity of all the surfaces presented in Fig. 3.

Like in the case of CO_{ads} oxidation (Fig. 2), the positive potential limit during the cycling of bulk Pt electrode strongly influences the HCOOH oxidation kinetics. Dia-

grams in Fig. 3a and b clearly show that the reaction rate is higher and the poisoning by CO_{ads} is lower on Pt cycled in the narrower potential window. This can be attributed to the change in the preferential crystal plane on the surface of polycrystalline Pt over the potential cycling in the extended potential window. Namely, Kita and Lei [33] compared HCOOH oxidation at three low-index Pt planes and demonstrated that Pt(111) is the least prone to the poisoning by CO_{ads} and the mostly active at low potentials. On the other hand, potential cycling of Pt(111) with the extended positive potential limit induce the reconstruction of the surface [34, 35]. Accordingly, decrease in the fraction of Pt (111) on the polycrystalline surface of Pt, both bulk Pt and Pt skeleton Pt_3Co structure (Fig. 3b), resulted in the lower activity and higher degree of poisoning by CO_{ads} in comparison to the Pt and Pt_3Co surfaces not previously exposed to the surface reconstruction.

Polarization curves for the HCOOH oxidation recorded under the quasi steady-state conditions going in the positive potential direction are presented in the form of Tafel plots in Fig. 4. The order in the activity of the electrodes is the same as determined under the potentiodynamic conditions. The enhancement factor of Pt_3Co alloy versus bulk Pt at 0.4 V is about 7. The Tafel slope for bulk Pt is ~0.18 V dec^{-1} in the potential region between 0.2 and 0.55 V, while for Pt_3Co alloy is ~0.16 V dec^{-1} in the region between 0.22 and 0.4 V. Both values imply high surface coverage by CO_{ads} [7, 11, 32].

Comparison between the HCOOH reaction rate on the Pt bulk electrodes after two different pretreatment procedures on Pt_3Co alloy and Pt skeleton Pt_3Co structure enable us to discuss the influence of Co on the Pt activity. Since Pt skeleton Pt_3Co structure has no Co atoms on the surface, the only possible effect is the electronic modification of Pt by the Co atoms beneath the surface Pt layer. Since the activity of Pt skeleton is only slightly higher than that of bulk Pt (Figs. 3b and 4b), it can be concluded that the electronic effect is not significant. In the case of Pt_3Co alloy and bulk Pt, except electronic effects, bifunctional mechanism and the ensemble effect might be operative. Although bifunctional effect cannot be excluded because CO_{ads} stripping peak on Pt_3Co alloy is negatively shifted with respect to the peak on bulk Pt, those peaks are positioned at 720 and 740 mV, which cannot produce any effect on HCOOH oxidation rate at the potentials below ~0.65 V (Fig. 2a). Besides, the peaks at the HCOOH potentiodynamic curves originating in the HCOOH oxidation on the Pt freed from CO_{ads} are positioned at the same potential (Fig. 3a). Therefore, higher activity of Pt_3Co alloy than bulk Pt electrode is to be ascribed mostly to the ensemble effect. This can be proved by the contrasting data of Pt–Au surfaces on which only ensemble effect is operative [11] with the data on Pt_3Co alloy. The enhancement factor of

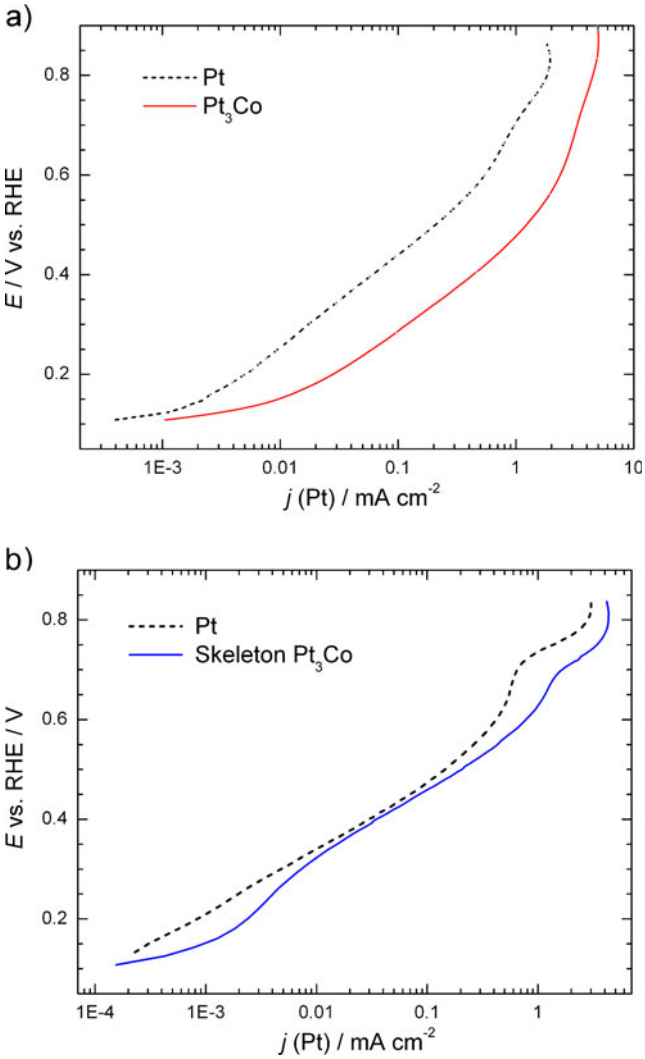

Fig. 4 Quasi steady-state polarization curves for the oxidation of HCOOH in 0.1 M $HClO_4$+0.5 M HCOOH electrolyte on **a** bulk Pt and Pt_3Co alloy and on **b** bulk Pt and Pt skeleton Pt_3Co structure, recorded in the positive-going sweeps at the rate of 1 mV s^{-1}. Current densities are referred to Pt surface

Pt_3Co over Pt of 7 was found in the quasi steady-state measurements at 0.4 V (Fig. 4a) and, according to Fig. 5 in [11], it corresponds to the Pt fraction of 0.82. This is close to the nominal Pt fraction of 0.75 in Pt_3Co alloy, especially having in mind that some chemical dissolution of Co from the alloy surface in the acid environment is possible.

Voltammetry of Pt_3Co/C and PtCo/C catalysts

Steady-state cyclic voltammograms of Pt_3Co/C, PtCo/C, and Pt/C catalysts in 0.1 M $HClO_4$ are presented in Fig. 5. As on bulk Pt and Pt_3Co alloy, hydrogen adsorption/desorption peaks are well resolved on Pt/C but not at the alloy catalysts. Formation of Pt oxide on Pt_3Co/C and PtCo/C catalysts is delayed with respect to Pt/C.

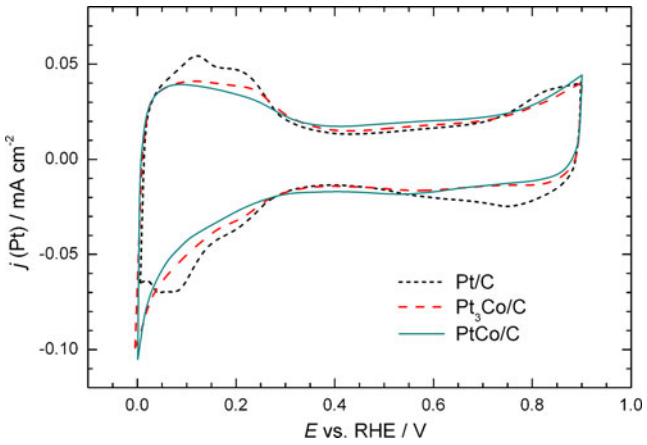

Fig. 5 Cyclic voltammograms of the supported nanosized catalysts Pt/C, Pt_3Co/C, and PtCo/C recorded in 0.1 M $HClO_4$ at the sweep rate of 50 mV s^{-1}

Oxidation of CO_{ads} on Pt_3Co/C and PtCo/C catalysts

Oxidation of preadsorbed CO is examined at the same catalysts, and the stripping voltammograms are given in Fig. 6. As one can see, the oxidation of CO_{ads} starts earlier on the Pt–Co nanoparticles than on pure Pt nanoparticles. This result and the delayed formation of Pt oxide on the Pt–Co alloy nanoparticles suggest that the bonds between CO or OH species and Pt atoms in alloys are weaker than the bond with Pt atoms on the pure Pt nanoparticles.

Analogously to the results on Pt_3Co bulk alloy and bulk Pt, the difference in the onset and the peak potential of CO_{ads} oxidation could be ascribed to the bifunctional effect and electronic modification of Pt by Co atoms. However, Pt_3Co, PtCo, and Pt nanoparticles used in the experiments presented in Fig. 6 were not of the same size, thus the particle size effect has also to be considered. In Pt/C catalyst the Pt particles are 2.5±0.2 nm in diameter [36], while Pt–Co particles are larger—the diameters of Pt_3Co and PtCo particles are 3.4±0.7 and 4.4±0.7 nm, respectively [23]. The position of the CO_{ads} stripping peaks, as seen in Fig. 6, follows the same order as the particle size, being more positive for the smaller particles. Moreover, the peak potential for CO_{ads} stripping on bulk Pt electrode is 0.74 V (Fig. 2a), while on Pt nanoparticles is 0.81 V, confirming the particle size effect in the adsorption of CO on Pt surfaces. Regarding OH adsorption, since no significant difference in OH adsorption was found between bulk Pt_3Co alloy and bulk Pt, the effect found on nanoparticles is likely to be caused by the different particle size.

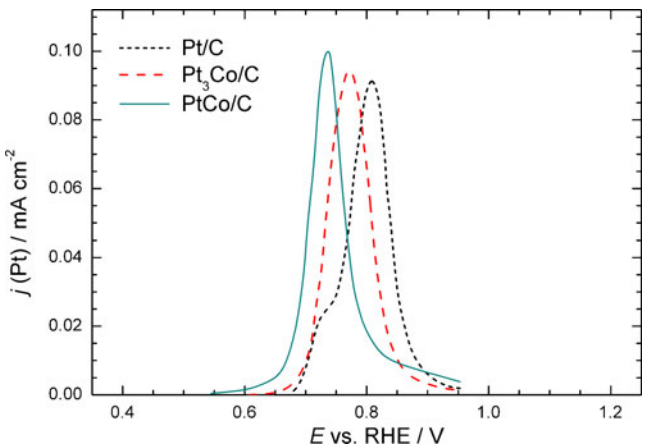

Fig. 6 CO_{ads} stripping voltammograms on the supported nanosized catalysts Pt/C, Pt_3Co/C, and PtCo/C in 0.1 M $HClO_4$ recorded at the sweep rate of 20 mV s^{-1}. Current densities are referred to Pt surface

The particle size effect in the adsorption of small adsorbates arises from the different d-band center of low and high coordinated atoms on the adsorbent surface. The low coordinated atoms, which are more abundant on the surfaces of small particles, have narrower d-band because of lower degree of overlapping between the atomic orbitals. The narrowing of the d-band increases the energy of the d-band center and, consequently, leads to stronger bond with the adsorbates [37]. Lower peak potential for CO_{ads} stripping on bulk Pt than on nanosized Pt particles [38] or on Pt monolayers [39] and positive shift in peak potential with the decrease in Pt nanoparticle diameter [40, 41] are well documented in literature.

Oxidation of formic acid on Pt_3Co/C and PtCo/C catalysts

Potentiodynamic polarization curves of HCOOH oxidation on Pt_3Co/C and PtCo/C catalysts are compared to Pt/C in Fig. 7. At the bimetal catalysts, HCOOH oxidation

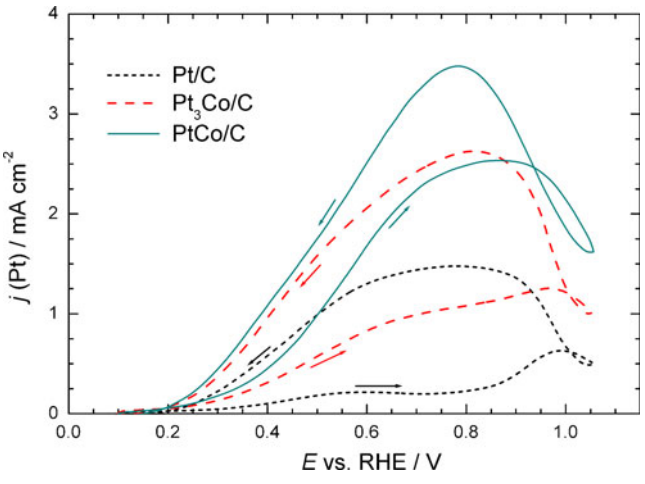

Fig. 7 Potentiodynamic polarization curves for the oxidation of HCOOH in 0.1 M $HClO_4$+0.5 M HCOOH electrolyte recorded on the supported nanosized catalysts Pt/C, Pt_3Co/C, and PtCo/C. Sweep rate 50 mV s^{-1}. Current densities are referred to Pt surface

commences earlier and the current densities are higher than at Pt, the effect being more pronounced for PtCo/C than for Pt_3Co/C. The increase of the current at ~0.85 V, which is ascribed to the HCOOH oxidation on the surface freed from CO_{ads}, is well expressed at the curve for Pt/C, barely seen at the curve for Pt_3Co/C and absent from the curve for PtCo/C. Accordingly, the surface poisoning by CO_{ads} is reduced in the presence of Co in the catalyst, especially in the case of PtCo/C. However, this does not mean that CO_{ads} formation is completely suppressed, because if the reaction takes place solely through the direct path, the HCOOH oxidation current will rise more steeply from the onset potential and reach the maximum already at ~0.5 V, as it was established for Pt–Au surface with 28% of Pt [11].

When Pt_3Co/C and PtCo/C were subjected to the prolonged potential cycling in order to leach Co from the surface of the nanoparticles, the polarization curves of HCOOH oxidation gained the same shape as for Pt/C. These experiments support the assumption that Co atoms beneath Pt surface have no significant effect on Pt electrochemical activity, i.e., that the promotion of the HCOOH reaction rate on Pt–Co surfaces originates predominantly in the ensemble effect. This explains why pristine Pt_3Co/C is less active than pristine PtCo/C—fraction of Co on the Pt_3Co surface is too low to produce significant ensemble effect.

Tafel plots constructed from the quasi steady-state polarization curves recorded in the positive-going potential sweeps are presented in Fig. 8. The order in activity follows the results under the potentiodynamic conditions: PtCo/C> Pt_3Co/C>Pt/C.

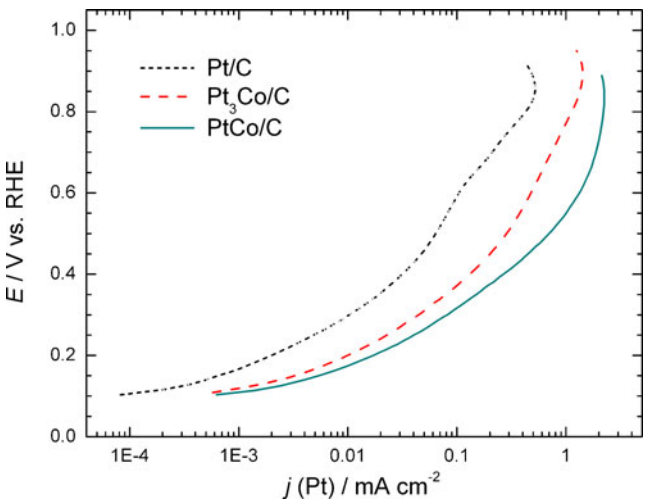

Fig. 8 Quasi steady-state polarization curves for the oxidation of HCOOH in 0.1 M $HClO_4$+0.5 M HCOOH electrolyte on the supported nanosized catalysts Pt/C, Pt_3Co/C, and PtCo/C recorded in the positive-going sweeps at the rate of 1 mV s^{-1}. Current densities are referred to Pt surface

The finding that after leaching of Co from the surface of Pt–Co nanoparticles their activity for HCOOH oxidation equals to the activity of pure Pt indicates that Pt–Co alloys are not viable anode electrocatalysts for DFAFC, because leaching of Co is inevitable during the long-term fuel cell operation.

Summary and conclusions

Bulk and nanosized Pt–Co alloys were investigated by cyclic voltammetry and CO_{ads} stripping voltammetry in order to establish whether Co atoms modify adsorption characteristics of Pt. It was found that for a valid comparison of the voltammograms, it is important to pretreat the Pt and Pt–Co alloys by the potential cycling in the same potential window because of the reconstruction of the Pt surface over the cycling.

When the cyclic voltammograms of the Pt_3Co alloy with Pt skeleton structure were compared to those of bulk Pt, no significant difference in the Pt-oxide formation and reduction was observed. Regarding hydrogen adsorption, the voltammetric peaks of strongly adsorbed hydrogen were the same at both electrodes, while peaks of weakly adsorbed hydrogen were slightly reduced on the Pt skeleton. Therefore, the electronic modification of Pt by Co atoms is not unambiguously confirmed by our cyclic voltammetry measurements of Pt_3Co alloy with Pt skeleton structure.

The oxidation of CO_{ads} on bulk Pt_3Co was negatively shifted for ~30 mV with respect to the same reaction on bulk Pt. However, when CO_{ads} stripping voltammograms on Pt_3Co alloy with Pt skeleton structure and on bulk Pt were contrasted, the difference was minor, i.e., on Pt skeleton the oxidation of CO_{ads} starts ~10 mV earlier than on bulk Pt. These results show that the influence of Co atoms is more pronounced if they are on the surface facing the electrolyte than if they are beneath the Pt skeleton, suggesting stronger effect of the oxidative removal of CO_{ads} by the oxygen-containing species adsorbed on oxophilic Co atoms than the effect of electronic modification of Pt by Co atoms.

Bimetallic Pt–Co surfaces express moderate promotion of the HCOOH oxidation kinetics with respect to pure Pt and lower degree of poisoning by CO_{ads}, which are mostly attributed to the ensemble effect. The enhancement factor of 7 found for bulk Pt_3Co alloy over bulk Pt at 0.4 V matches pretty well to the pure ensemble effect established for Pt–Au surface of the same Pt fraction [11]. Similarly to the CO_{ads} oxidation, Pt_3Co alloy with Pt skeleton structure was found to be just a slightly more active for HCOOH oxidation than bulk Pt, confirming low electronic effect of Co on Pt in the skeleton structure.

Acknowledgment This work was financially supported by the Ministry of Science and Technological Development, Republic of Serbia, Contract No. 172060.

References

1. Yu X, Pickup PG (2008) J Power Sourc 182:124
2. Capon A, Parsons R (1973) J Electroanal Chem 44:1
3. Miki A, Ye S, Osawa M (2002) Chem Commun 1500–1501
4. Neurock M, Janik M, Wieckowski A (2009) Faraday Discuss 140:363
5. Cuesta A, Escudero M, Lanova B, Baltruschat H (2009) Langmuir 25:6500
6. Scheijen FJE, Beltramo GL, Hoeppener S, Housmans THM, Koper MTM (2008) J Solid State Electrochem 12:483
7. Park IS, Lee KS, Choi JH, Park HY, Sung YE (2007) J Phys Chem C 111:19126
8. Kristian N, Yu Y, Gunawan P, Xu R, Deng W, Liu X, Wang X (2009) Electrochim Acta 54:4916
9. Patra S, Das J, Yang H (2009) Electrochim Acta 54:3441
10. Choi JH, Park KW, Park IS, Kim K, Lee JS, Sung YE (2006) J Electrochem Soc 153:A1812
11. Obradović MD, Tripković AV, Gojković SL (2009) Electrochim Acta 55:204
12. Xia X, Iwasita T (1993) J Electrochem Soc 140:2559
13. Alden LR, Han DK, Matsumoto F, Abruña HD, DiSalvo FJ (2006) Chem Mater 18:5591
14. Casado-Rivera E, Gál Z, Angelo ACD, Lind C, DiSalvo FJ, Abruña HD (2003) Chem Phys Chem 4:193
15. Tripković AV, Popović KDJ, Stevanović RM, Socha R, Kowal A (2006) Electrochem Commun 8:1492
16. Chetty R, Scott K (2007) J New Mater Electrochem Syst 10:135
17. Gojković SLJ, Tripković AV, Stevanović RM, Krstajić NV (2007) Langmuir 23:12760
18. Rice C, Ha SY, Masel RI, Wieckowski A (2003) J Power Sourc 115:229
19. Thomas FS, Masel RI (2004) Surf Sci 573:169
20. Kitchin JR, Nørskov JK, Barteau MA, Chen JG (2004) J Chem Phys 120:10240
21. Kitchin JR, Nørskov JK, Barteau MA, Chen JG (2004) Phys Rev Lett 93:156801
22. Stamenkovic V, Schmidt TJ, Ross PN, Markovic NM (2002) J Phys Chem B 106:11970
23. Paulus UA, Wokaun A, Scherer GG, Schmidt TJ, Stamenkovic V, Radmilovic V, Markovic NM, Ross PN (2002) J Phys Chem B 106:4181
24. Wakisaka M, Mitsui S, Hirose Y, Kawashima K, Uchida H, Watanabe M (2006) J Phys Chem B 110:23489
25. Bogdanovskaya VA, Tarasevich MR, Reznikova LA, Kuznetsova LN (2010) Russ J Electrochem 46:1011
26. Xu Q, Kreidler E, He T (2010) Electrochim Acta 55:7551
27. Stamenkovic VR, Mun BS, Mayrhofer KJJ, Ross PN, Markovic NM (2006) J Am Chem Soc 128:8813
28. Kinoshita K, Stonehart P (1975) Electrochim Acta 20:101
29. Papadimitriou S, Tegou A, Pavlidou E, Armyanov S, Valova E, Kokkinidis G, Sotiropoulos S (2008) Electrochim Acta 53:6559
30. Tegou A, Papadimitriou S, Kokkinidis G, Sotiropoulos S (2010) J Solid State Electrochem 14:175
31. Wakisaka M, Suzuki H, Mitsui S, Uchida H, Watanabe M (2008) J Phys Chem C 112:2750
32. Lović JD, Tripković AV, Gojković SLJ, Popović KDJ, Tripković DV, Olszewski P, Kowal A (2005) J Electroanal Chem 581:294
33. Kita H, Lei HW (1995) J Electroanal Chem 388:167
34. Jerkiewicz G, Vatankhah G, Lessard J, Soriaga MP, Park YS (2004) Electrochim Acta 49:1451
35. Björling A, Ahlberg E, Feliu JM (2010) Electrochem Commun 12:359
36. Esparbé I, Brillas E, Centellas F, Garrido JA, Rodríguez RM, Arias C, Cabot PL (2009) J Power Sourc 190:201
37. Hammer B, Nielsen OH, Nørskov JK (1997) Catal Lett 46:31
38. Cherstiouk OV, Simonov PA, Savinova ER (2003) Electrochim Acta 48:3851
39. Kumar S, Zou S (2007) Langmuir 23:7365
40. Takasu Y, Iwazaki T, Sugimoto W, Murakami Y (2000) Electrochem Commun 2:671
41. Guerin S, Hayden BE, Lee CE, Mormiche C, Owen JR, Russell AE, Theobald B, Thompsett D (2004) J Comb Chem 6:149